Materials Science & Engineering A 626 (2015) 263–274

Contents lists available at ScienceDirect

Materials Science & Engineering A

journal homepage: www.elsevier.com/locate/msea

An analysis of small punch creep behaviour in the γ titanium aluminide Ti–45Al–2Mn–2Nb

R.J. Lancaster [a,*], W.J. Harrison [b], G. Norton [a]

[a] Institute of Structural Materials, College of Engineering, Swansea University, Singleton Park, Swansea SA2 8PP, UK
[b] Materials Research Centre, College of Engineering, Swansea University, Singleton Park, Swansea SA2 8PP, UK

ARTICLE INFO

Article history:
Received 2 October 2014
Received in revised form
8 December 2014
Accepted 13 December 2014
Available online 23 December 2014

Keywords:
Titanium aluminide
Small punch
Creep
Finite element

ABSTRACT

Previous literature on gamma titanium alumindes (γ-TiAl) have found that this family of alloys offer significant potential for replacing more conventional nickel and titanium based alloy systems in future designs of gas turbine engines. Despite the inherent brittle nature of such materials, γ-TiAl typically exhibits considerable ductility at elevated temperatures and a demonstrable uniaxial creep response. Until now, the creep properties of γ-TiAl have primarily been sourced from conventional uniaxial approaches, which require significant material quantities in order to perform a full stress–temperature–life assessment. This is not always possible for new alloys where sufficient quantities of material are unavailable. The small punch (SP) creep test represents an attractive alternative to uniaxial creep testing since the volume of material required is much less. However, much of the current literature on SP testing is limited to the application of traditionally ductile materials. This paper assesses the suitability of the SP method to characterise the creep properties of γ-TiAl alloys. Finite element modelling has been used to characterise the SP deformation and rupture behaviour.

1. Introduction

Reducing structural weight is one of the main factors in reducing carbon emissions and improving aircraft performance. Lighter and/or stronger materials allow greater range and speed and may also contribute to reducing operational costs. Through extensive research stemming from the mid 1990s [1–3], titanium aluminides (TiAl) are now providing an attractive option for many jet engine components subjected to elevated temperatures, despite its inherent brittleness at ambient conditions [4]. TiAl is an intermetallic material that typically offers a superior high temperature performance compared with traditional titanium materials, but also a reduced density in relation to currently employed nickel base superalloys. There are several forms of TiAl that can be utilised for such applications, including γ-TiAl, alpha 2-Ti_3Al and $TiAl_3$ [5,6]. Amongst these variants, γ-TiAl has received much attention from the aerospace industry for low pressure turbine blades due to the attractive balance of mechanical properties that they possess [7]. γ-TiAl typically exhibits a low density, good corrosion resistance and high temperature strength comparable to conventional titanium alloys, whilst also offering a superior creep resistance at temperatures above 600 °C, the temperature at which Ti alloys are susceptible to oxidation damage [4,5].

A thorough characterisation of the creep properties of any modern alloy, such as γ-TiAl, can be an expensive and timely process and as such, significant effort is now being placed in identifying suitable alternative characterisation techniques. The small punch (SP) test is now widely regarded as an effective tool for ranking the creep properties of a number of critical structural materials from power plant components. The technique was developed around three decades ago as a method of assessing material degradation in nuclear pressure vessels and reactors. As such, the technique has proven to be successful on a number of material systems including aluminium and steels [8–11]. Over recent years, the SP creep test has become an attractive miniaturised mechanical test method ideally suited for situations where only a limited quantity of material is available for qualification testing. Typically, the method requires only a modest amount of material and can provide key mechanical property information for highly localised regions of critical components. One such example of the technique's applicability is the determination of the creep properties of heat affected zones (HAZ) of welded joints [12,13]. More recently, the SP creep test has been recognised for its unique potential in assessing the capabilities of novel materials for aero engine applications, where substantial quantities of experimental materials cannot easily be produced to allow characterisation

* Corresponding author. Tel.: +44 1792 295965.
E-mail address: r.j.lancaster@swansea.ac.uk (R.J. Lancaster).

http://dx.doi.org/10.1016/j.msea.2014.12.045
0921-5093/

through conventional mechanical test approaches [14]. This has become increasingly important in recent years where the continuous evolution of the jet engine has led to the need to develop new alloys to withstand the arduous temperature conditions experienced in service whilst offering a weight saving in order to improve engine efficiency, thus providing a major challenge to materials scientists and engineers who are now starting to re-evaluate the suitability of traditional alloy systems for structural parts. As such, SP creep testing offers a feasible option of determining the creep properties of novel alloy variants.

Effort has previously been made in correlating conventional creep results to data produced through SP testing by use of the k_{SP} approach [9,15]. The ability to correlate SP creep results with uniaxial creep data is an important factor when considering the advantages of the SP creep test technique, particularly in allowing for savings in test intensive material characterisation programmes. As previously mentioned, the correlation between SP loading and uniaxial stress can be achieved by employing the k_{SP} method, which is detailed in the European Code of Practice (CoP) for small punch testing [15]. The relationship behaves as follows:

$$\frac{F}{\sigma} = 3.33 k_{SP} R^{-0.2} r^{1.2} h_0 \quad (1)$$

where F is the SP load, σ is the stress applied in a uniaxial creep test, R is the radius of the receiving hole (2 mm), r is the radius of the punch indenter (1 mm) and h_0 is the test piece thickness (0.5 mm). This empirical relationship has been derived from membrane stretching theory where k_{SP} represents the creep ductility of the material and the method has been proven to be an effective means of correlating data produced through small punch testing to conventional uniaxial creep results. This correlative approach however, has thus far only been applied to inherently ductile materials.

The focus of this paper is to investigate the applicability of the SP creep test in determining the creep properties of inherently brittle materials, such as γ-TiAl alloys, compared to more conventional testing approaches. There are clear benefits in developing a robust, low-cost characterisation technique which may prove effective in the future lifing of current and next generation alloys.

2. Experimental methods

2.1. Materials

The study was carried out on the intermetallic γ-Ti–45Al–2Mn–2NbXD (exothermic dispersion) in the cast and hot isostatically pressed (HIP) condition with a fully lamellar microstructure, as shown in Fig. 1. The uniaxial creep behaviour of this material has previously been reported and analysed [4,16].

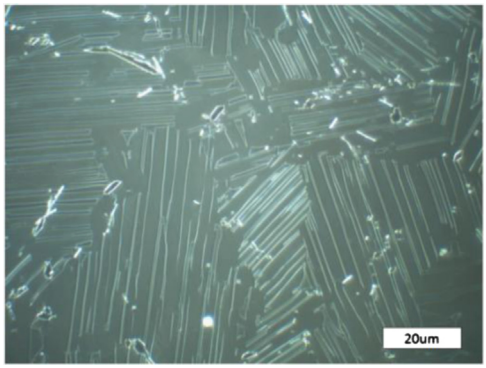

Fig. 1. Microstructure of cast and HIP'ed Ti–45Al–2Mn–2Nb(XD).

2.2. Specimens

The SP creep tests were performed on specimens, or miniature discs, conforming to the European Code of Practice (CoP) for small punch testing [15] with a diameter of 9.5 mm and a thickness of 500 ± 5 μm. Specimen preparation involved machining the discs to a thickness of ~700 μm followed by grinding in a specially designed holder to the final dimensions. Grinding was undertaken with progressively finer grit papers (to reduce surface effects) until the final finish was achieved with a 1200 grit fine paper as defined in the CoP [15]. A representative image of a miniature disc specimen and nominal dimensions is given in Fig. 2(a).

The uniaxial creep tests were performed on specimens machined from bar stock material, Fig. 2b. The dimensions within this design conform with the International standard for uniaxial creep testing, (ISO204:2009) [17] and the gauge section was ground finished to a diameter of 5.6 mm with a parallel gauge length of 28.0 mm.

3. Methods

A series of SP and uniaxial creep tests were performed in this programme under various applied load/stress values, at temperatures between 700 and 750 °C. SP creep tests were undertaken in a bespoke test rig, as shown in Fig. 3. In this arrangement, the miniature disc specimen is placed in a lower die holder, which locates the sample in the centre of the rig and applies a circumferential clamping load to hold the disc securely in place during loading. Load is then applied to the disc using a 2 mm diameter hemispherical ended Nimonic punch via a vertical ram that transmits the applied load through calibrated weights placed on the load pan. Heat is applied using a single zone furnace digitally controlled and constantly monitored throughout the test by two Type K thermocouples located in a drilled hole in the upper die, close to the surface of the disc. Two linear variable displacement transducers (LVDT) were employed at either end of the test frame to monitor the rate of displacement that the specimen undergoes during a test. The top transducer is located just below the load pan and monitors the displacement of the indenter penetrating into the top surface of the disc. The bottom transducer is located within the lower pull-rod and the measurement is taken directly from the disc via a quartz rod that is placed in direct contact with the underside of the sample. This enables monitoring of the average deflection experienced as the specimen starts to deform under an applied load. The resulting time–displacement data are recorded at regular intervals depending on the rate of deformation using a dedicated PC based data logging system.

Uniaxial creep specimens were tested in tension under constant stress according to the International standard ISO204:2009 [17]. All tests were performed in an air environment with heating provided by a three-zone furnace. Temperature was monitored along the gauge length using calibrated R type thermocouples, located with intimate contact to the specimen surface. Creep elongation was recorded using a parallel extensometer cage system that is clamped to the 'ridged' locations of the gauge section, and monitored using two high precision LVDTs.

4. Results

The typical load–displacement relationship for an SP creep test is presented in Fig. 4(a) where the graph shows the displacement behaviour for a γTi–45Al–2Mn–2Nb(XD) specimen tested at 750 °C under a load of 235 N. The resultant curve displays an initial decaying displacement rate followed by a steady state period of deformation before the rate of displacement accelerates through

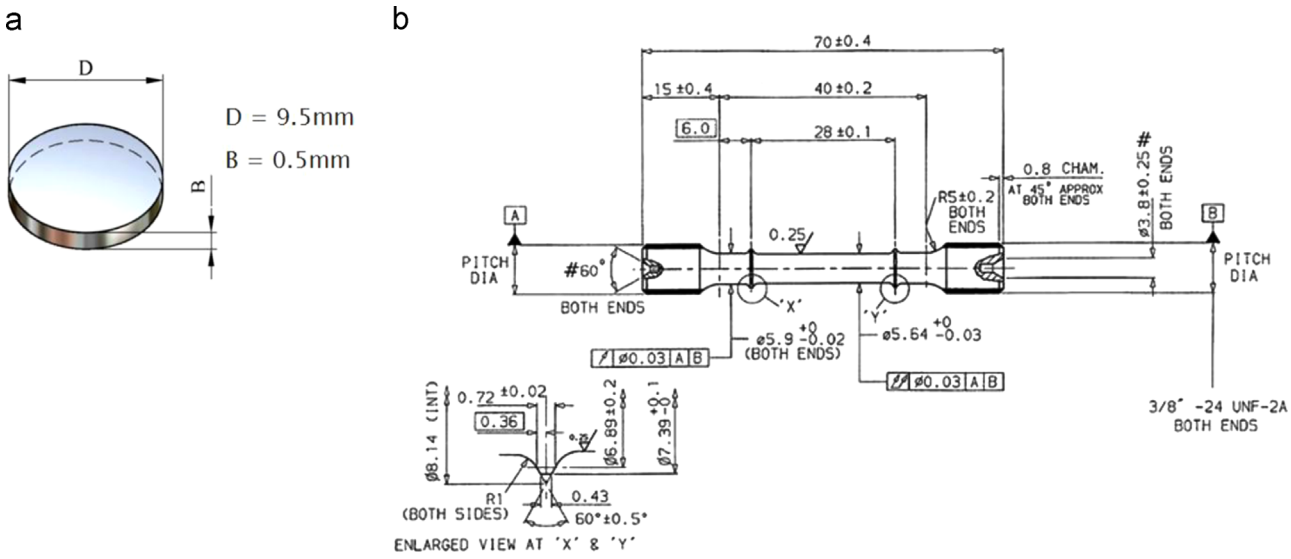

Fig. 2. (a) Small punch miniature disc specimen and (b) uniaxial creep specimen dimensions.

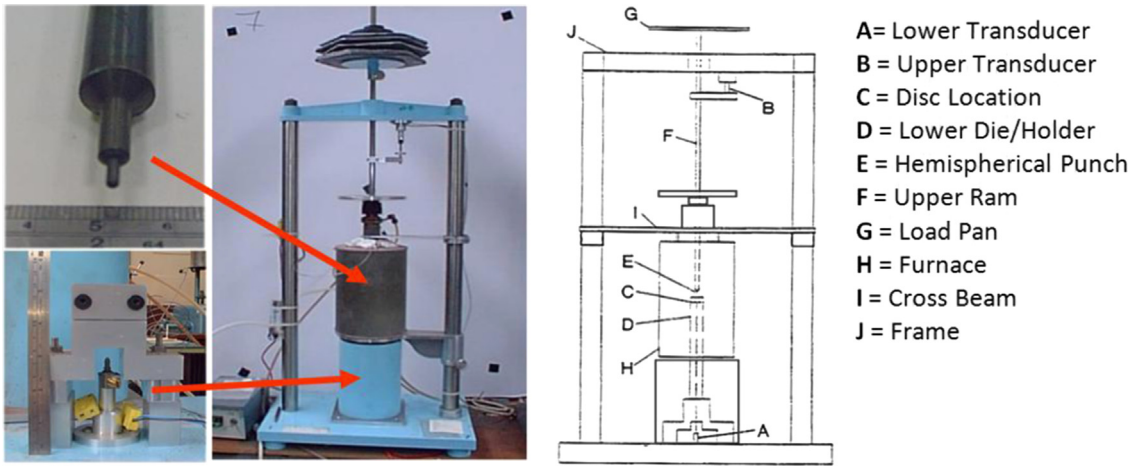

Fig. 3. Small punch creep test rig facility.

to failure. This behaviour is comparable with that typically expected for a conventional uniaxial creep test where a material will usually deform with decreasing rate during primary creep, followed by a tertiary phase during which creep rate increases (Fig. 4(b)). However, even though the two test methods appear to produce a similar creep response on a given material, in reality, the deformation behaviour is quite different. In a SP creep test, the miniature disc sample is subjected to an initial period of compressive loading, followed by a bending motion and finally a stage of tensile elongation. The compressive loading occurs as the punch tip impacts the upper surface of the disc sample, leading to a stage where the membrane around the tip begins to stretch. From here, the membrane deforms and thinning occurs under a biaxial stress condition. As such the initial bending and biaxial loading observed in this test approach contrasts to the deformation behaviour experienced in a conventional creep test arrangement where the specimen simply elongates under an applied uniaxial tensile load.

A series of SP experiments were performed at 700 and 750 °C in order to determine the sensitivity of SP testing in establishing differences in applied load and temperature. Fig. 5 illustrates the differences in time–displacement for the SP tests at 750 °C under a range of applied loads. As can be seen, the shape of the curve changes in relation to the load applied in a similar manner to that observed in traditional uniaxial tests, where the highest load test (260 N) fails the earliest, followed shortly after by the 235 N test and so on. In each case, the discs failed through cracking followed by penetration of the punch. The influence of load is also reflected in the amount of displacement observed in the primary deformation of each test, where the highest load experiences the largest amount of primary displacement and the lowest load the smallest. There is little doubt that the SP tests clearly differentiate the load dependence of γ-TiAl and a similar response is observed in relation to temperature. Fig. 6 displays the time to rupture lives for the SP tests performed at 700 and 750 °C and it is evident that the tests undertaken at the lower temperatures exhibit a superior response.

It has previously been documented that during SP deformation in a ductile material, failure typically occurs around the periphery of the punch indentation where thinning of the miniature disc is usually observed prior to rupture. As such, a partly hinged ligament or 'cap' tends to develop from the thinned region that can often detach itself from the bulk material [18]. However, it is not clearly understood as to whether the deformation behaviour of a more inherently brittle alloy is similar to that of a ductile material. To characterise the SP creep deformation of a γ-TiAl disc, a series of interrupted tests were performed to capture the fracture behaviour at different stages of a typical SP test. A consistent test condition was employed, where the tests were performed at 750 °C and an applied load of 235 N, with the various experiments interrupted at

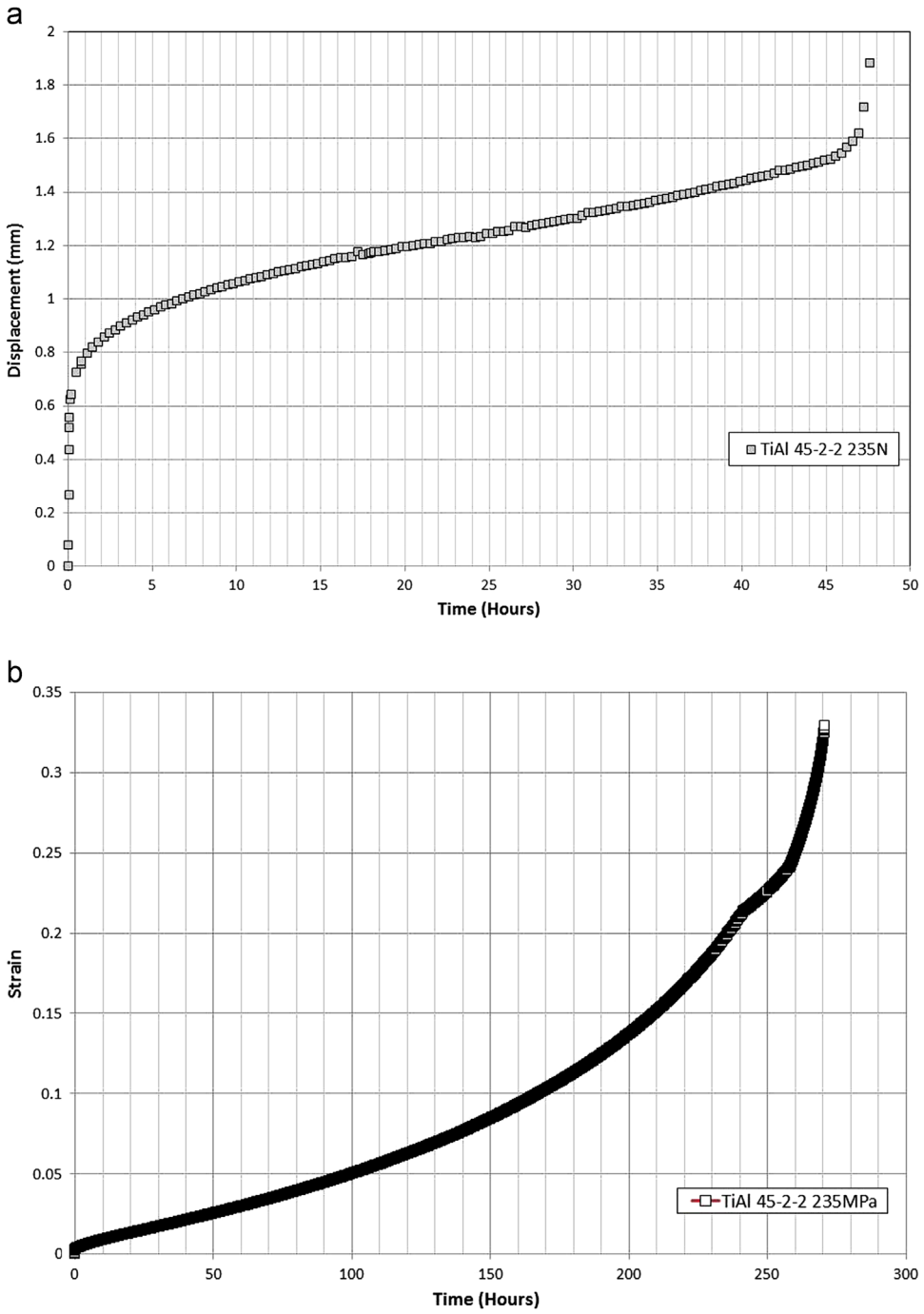

Fig. 4. Typical γ-TiAl 45-2-2(XD) creep curves of (a) displacement–time behaviour for an SP creep test (750 °C, 235 N) and (b) strain–time behaviour for a uniaxial creep test (750 °C, 235 MPa).

1/4 life, 1/2 life and after final rupture. Fractographic images from these tests are displayed in Fig. 7(a–e). Fig. 7(a) illustrates that cracking is observed on the underneath of the disc specimen after a relatively short period of time (1/4 life). The cracks then grow in a radial fashion from the central region of the disc and as time progresses, the cracks become more extensive as the stretched membrane of material becomes unable to withstand the applied load until final rupture occurs. As such, this mechanism of crack growth is considerably different to that seen in ductile materials.

From these results, additional interrupted tests were performed in order to determine the full extent of the brittle cracking behaviour in a γ-TiAl disc. The first test was carried out at 750 °C under a load of 213 N and stopped immediately as the total displacement reached 0.4 mm. The time period to achieve this level of displacement was 90 s, and from here, the specimen was removed and fractographic analysis revealed that radial cracking was indeed present. A second test was then undertaken with similar test conditions, in an attempt to capture the onset of cracking at an earlier stage. The test was stopped immediately after the load was applied, and post-test analysis once again revealed brittle radial cracking.

4.1. k_{SP} Correlation

As previously mentioned, the k_{SP} approach (Eq. 1), as defined in the CoP [15], has previously been used to correlate small punch

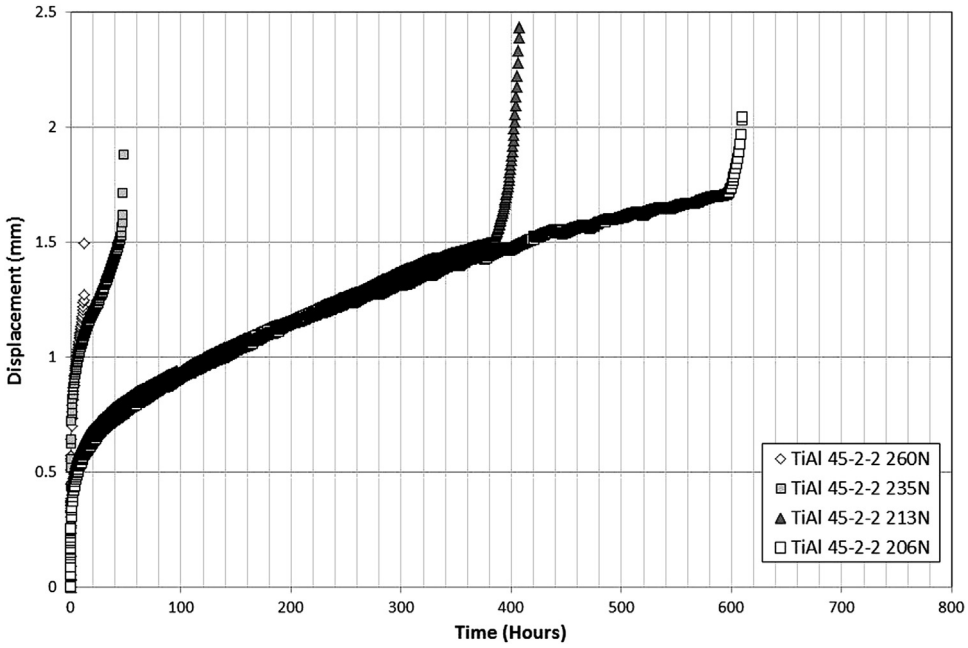

Fig. 5. Displacement–time curves for SP creep tests on γ-TiAl 45-2-2(XD) at 750 °C.

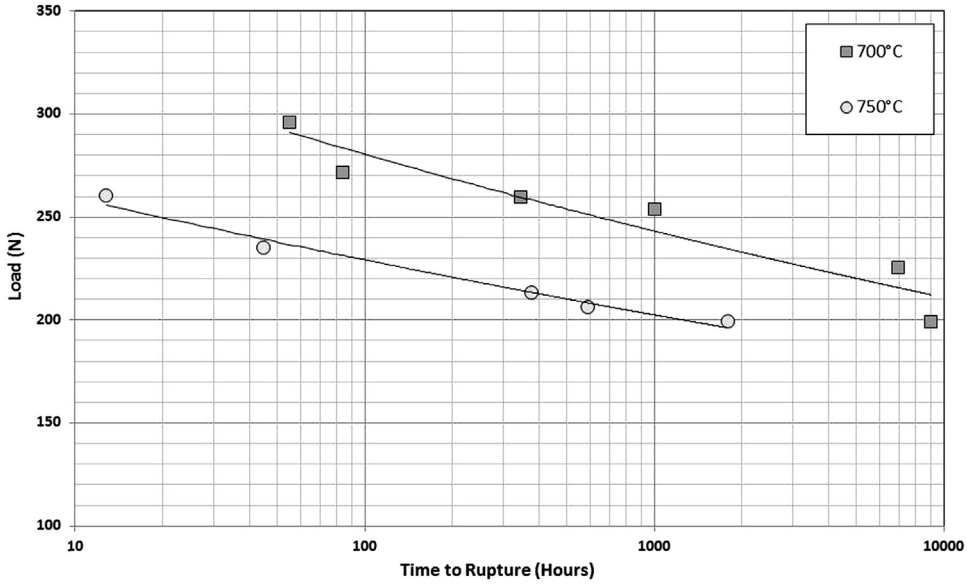

Fig. 6. Load–time to rupture behaviour for SP creep tests on γ-TiAl 45-2-2(XD) at 700 and 750 °C.

and uniaxial creep data for a particular material. The relationship is derived from membrane stretching theory but remains empirical in nature due to the incorporation of a material constant, given here as k_{SP}. When no uniaxial data is readily available for a direct comparison, k_{SP} is usually referred to as 1. In such a scenario however, the method can only serve as a rough approximation of the corrected creep stress. As such, uniaxial creep data on γ-TiAl 45-2-2(XD) was gathered from a previous programme [4] and used in order to assess the suitability of the k_{SP} approach in correlating the data. An important point to consider is that each of the uniaxial tests were performed under constant stress, whereas the majority of previously reported comparisons were obtained from constant load tests. Furthermore, as shown in Fig. 7, cracking occurs early during SP testing and a rapid onset of failure, indicated by a sharp increase in rate immediately prior to rupture is observed (Fig. 5). As such, it was found that the SP and uniaxial results demonstrated notably different slopes when plotted as a stress–time to rupture relationship, as given in Fig. 8, thus illustrating the limitation of the approach. The k_{SP} factor acts to simply change the position of the results with respect to stress and is not capable of changing the gradient of the fit to produce a more accurate correlation of the different data sets.

4.2. A finite element model of the small punch creep test

The k_{SP} approach provides a simple correlation of comparing uniaxial creep lives to small punch creep data and has been proven to be effective for many materials. However, as seen for this alloy a more detailed analysis is required. Finite element models have been previously used to predict SP creep behaviour in the ferritic

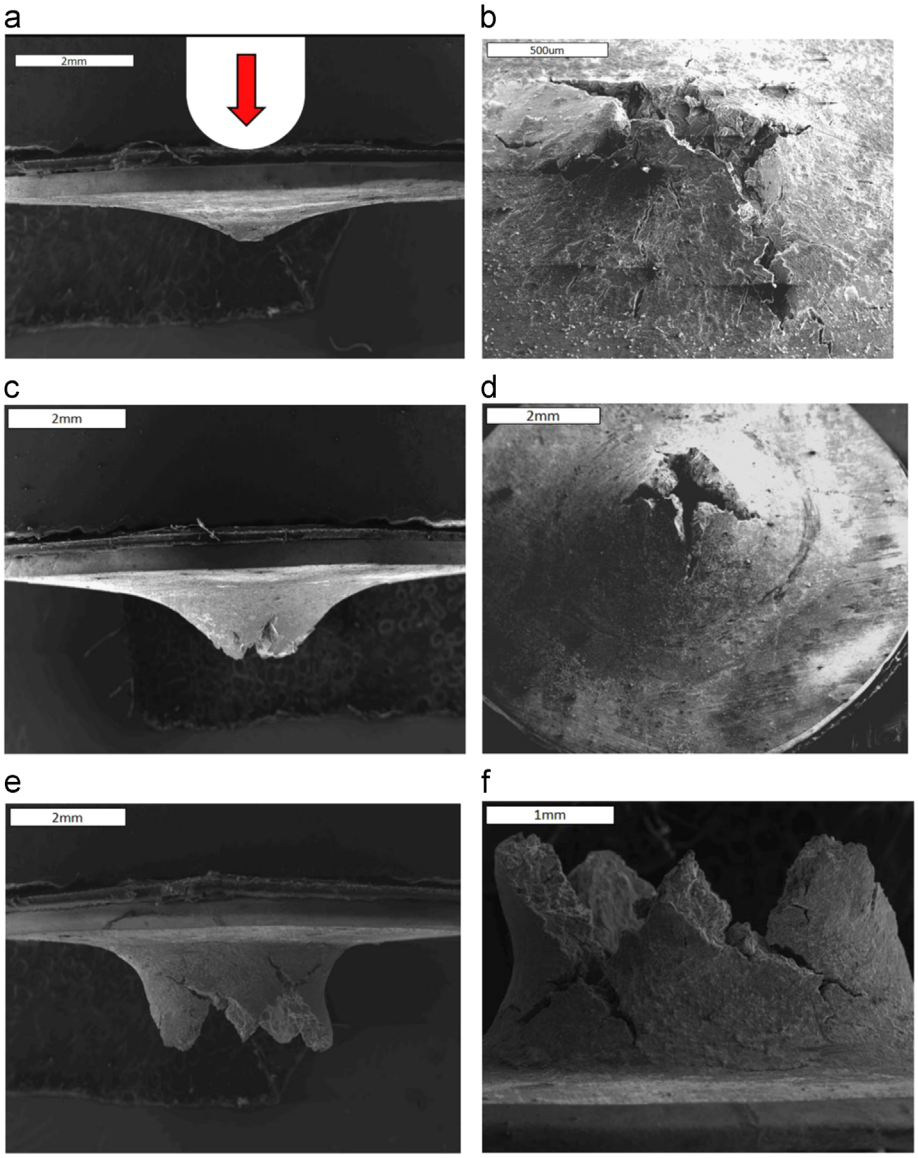

Fig. 7. SEM fractography of SP creep test on γ-TiAl 45-2-2(XD) (750 °C, 235 N). (a) Side view of disc at 1/2 life with representation of punch indenter, (b) underneath of disc at 1/4 life, (c) side view of disc at 1/2 life, (d) Underneath of disc at 1/2 life, (e) side view of disc after final rupture, and (f) underneath of disc after final rupture.

steels [19] and aluminium alloys [20] using models based on uniaxial creep data. Comparing predicted SP behaviour to that observed experimentally allows confidence in understanding the mechanism(s) of SP creep in the relevant alloy. To predict SP creep in γ-Ti–45Al–2Mn–2Nb a suitable creep model is required. One such model has been previously described [16] which uses the theta (θ) projection technique to relate creep behaviour to test conditions. This model also predicts creep rupture based on the accumulation of creep damage (W). A constitutive creep model based on the θ – projection technique was developed by Evans [21] and this has been incorporated into the commercially available solver Abaqus using a *CREEP subroutine. This method offers the benefit of relating creep rate to the accumulation of internal material state variables representing dislocation hardening (H), recovery (R) and internal creep damage (W) which has been show to predict creep behaviour better than strain or time based hardening methods for cases where stress evolves greatly over time [22]. Using this method, the instantaneous creep rate can be calculated based on the current state of the material characterised by H, R and W and the initial effective creep rate for the virgin material, $\dot{\bar{\varepsilon}}_0$. The rate of accumulation of the state variables can be related to creep strain using the proportionality constants $\hat{H}$, $\hat{R}$ and $\hat{W}$, where

$$\dot{H} = -\hat{H}\dot{\varepsilon} \tag{2}$$

$$\dot{R} = \hat{R} \tag{3}$$

$$\dot{W} = \hat{W}\dot{\varepsilon} \tag{4}$$

$\dot{\bar{\varepsilon}}_0$, $\hat{H}$, $\hat{R}$ and $\hat{W}$ are functions of stress and temperature and can be derived from the θ-coefficients using

$$\dot{\bar{\varepsilon}}_0 = \theta_1\theta_2 + \theta_3\theta_4 \tag{5}$$

$$\hat{H} \equiv \frac{\theta_2}{\theta_1\theta_2 + \theta_3\theta_4} \tag{6}$$

$$\hat{R} \equiv \frac{\theta_2\theta_3\theta_4}{\theta_1\theta_2 + \theta_3\theta_4} \tag{7}$$

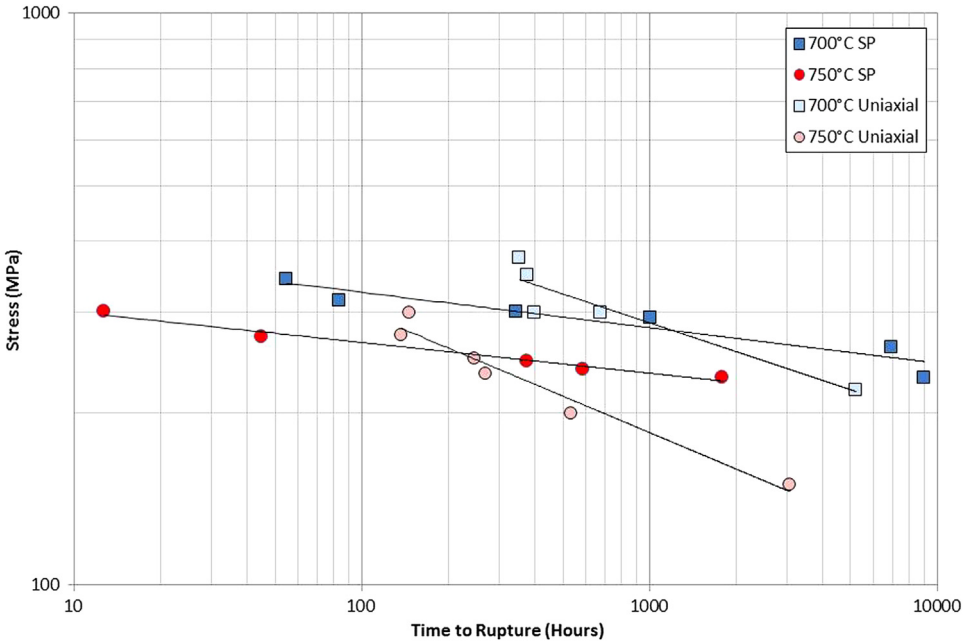

Fig. 8. k_{SP} correlation for uniaxial and converted SP data for γTiAl 45-2-2(XD) at 700 and 750 °C (k_{SP}=0.8).

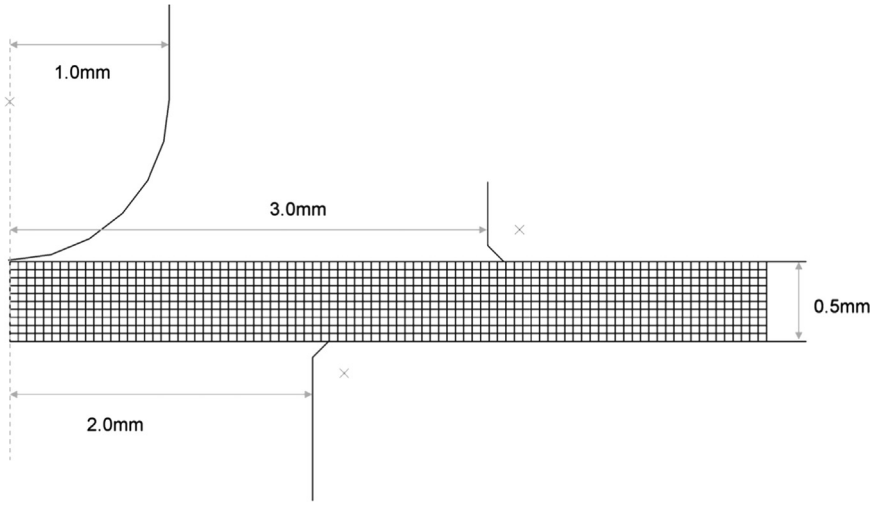

Fig. 9. Geometry of the SP creep model.

Table 1
Values of A_k and n_k for Ti–45Al–2Mn–2Nb [16].

θ	A	n
1	0.016631	0.948228
2	1.8×10^{14}	4.940382
3	0.090096	0.883272
4	6.14×10^{12}	4.473413

$$\hat{W} \equiv \frac{1}{\theta_3} \tag{8}$$

Assuming creep damage is a tertiary process, effective creep rate $\dot{\bar{\varepsilon}}$ can be calculated using

$$\dot{\bar{\varepsilon}}^{cr} = \dot{\bar{\varepsilon}}_0^{cr}\left(1+H+R+\frac{\hat{R}}{\hat{H}\dot{\bar{\varepsilon}}_0}W\right) \tag{9}$$

The state variables can then be updated for the next increment $(i+1)$ with a time of $(t+\delta t)$

$$H_{i+1} = H_i - \hat{H}\dot{\bar{\varepsilon}}_0(1+H_i+R_i)\partial t \tag{10}$$

$$R_{i+1} = R_i + \hat{R}\partial t \tag{11}$$

$$W_{i+1} = W_i + \frac{\hat{W}\hat{R}}{\hat{H}}(1+W_i)\partial t \tag{12}$$

The theta coefficients, θ_{1-4} can be calculated from von-Mises stress, $\bar{\sigma}$, and temperature, T, using the functions

$$\theta_1 = A_1\left(\frac{\sigma}{\sigma_{TS}}\right)^{n_1} \tag{13}$$

$$\theta_2 = A_2\left(\frac{\sigma}{\sigma_{TS}}\right)^{n_2}\exp\left(\frac{-Q_2^*}{RT}\right) \tag{14}$$

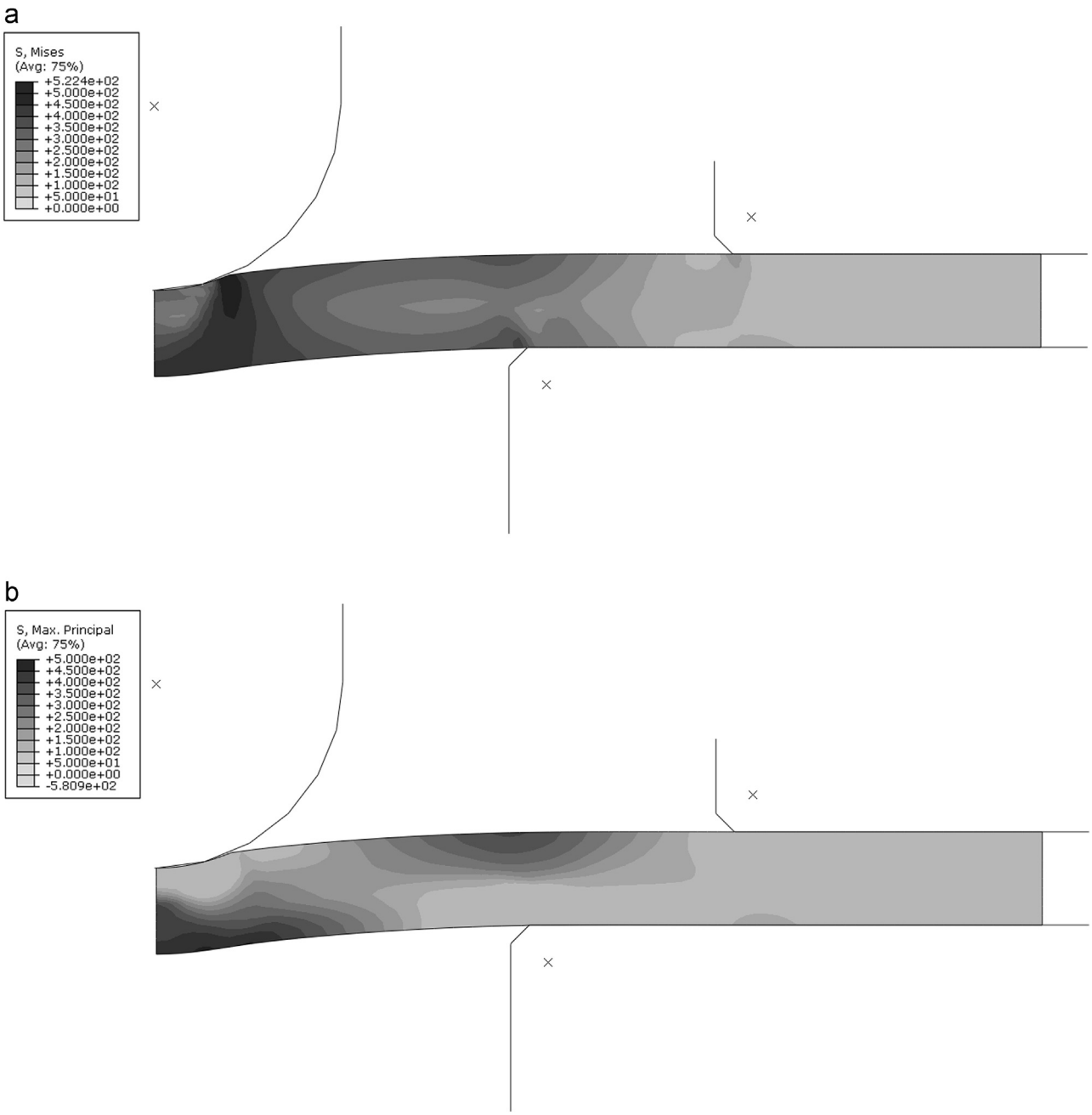

Fig. 10. Predicted (a) von-Mises and (b) maximum principle stress in the disc with a punch displacement of 0.2 mm and a punch load of 254 N (700 °C).

$$\theta_3 = A_3\left(\frac{\sigma}{\sigma_{TS}}\right)^{n_3} \tag{15}$$

$$\theta_4 = A_4\left(\frac{\sigma}{\sigma_{TS}}\right)^{n_4}\exp\left(\frac{-Q_4^*}{RT}\right) \tag{16}$$

where n_{1-4} and A_{1-4} are material constants obtained from uniaxial constant stress creep tests [16] the values of which are given in Table 1. The activation energies Q_2^* and Q_4^* are both 330 JK^{-1} mol^{-1} and $R$is the universal gas constant (8.314 JK^{-1} mol^{-1}).

An axisymmetric model was used to predict deformation in a SP creep test with model geometries representing those of the experiment. The disc had a diameter of 9.5 mm and a thickness of 0.5 mm and was modelled using 900 axisymmetric CAX4 elements. The top and bottom surfaces of the clamp and the punch were modelled as rigid surfaces. The top and bottom clamp hole diameters were 6 mm and 4 mm respectively and the punch had a tip radius of 1 mm (Fig. 9). Rough contact was assumed between all contact pairs with a coefficient of friction of 0.35. Load was applied through the punch surface during an initial static step and held during a subsequent transient (∗visco) step.

4.3. Stress analysis of the SP creep test

Finite element analyses allow the stress field within the SP test specimen to be examined. Since the SP test is axisymmetric the global cylindrical coordinate system is used where r is the radial direction, z is the axial direction and θ is the circumferential direction. The von-Mises effective stress, $\bar{\sigma}$, for an axisymmetric

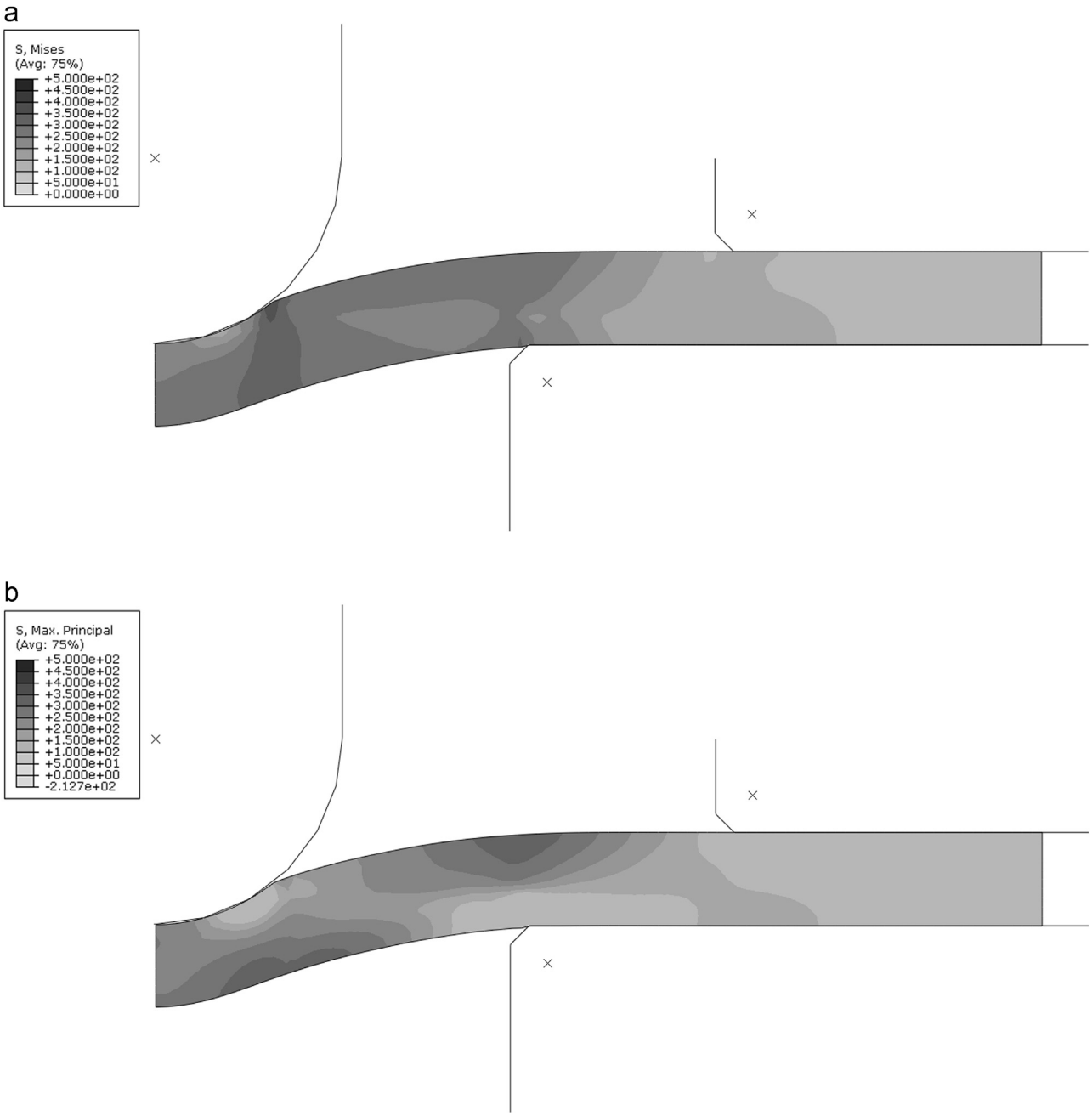

Fig. 11. Predicted (a) von-Mises and (b) maximum principle stress in the disc with a punch displacement of 0.5 mm and a punch load of 254 N (700 °C).

stress state can be calculated using

$$\overline{\sigma} = \sqrt{\frac{1}{2}\left[(\sigma_{zz}-\sigma_{rr})^2+(\sigma_{rr}-\sigma_{\theta\theta})^2+(\sigma_{\theta\theta}-\sigma_{zz})^2\right]+3\left(\sigma_{rz}^2\right)} \quad (17)$$

where σ_{zz}, σ_{rr} and $\sigma_{\theta\theta}$ are the axial, radial and hoop stresses respectively. σ_{rz} is the active shear stress, whereas $\sigma_{z\theta}$ and $\sigma_{\theta r}$ are inactive due to symmetry. The stress in the SP test is multiaxial and evolves throughout the test. Upon initial loading, there is a high compressive stress immediately adjacent to the punch with a high tensile (radial and hoop) stress observed on the lower side. The von-Mises stress is high across the thickness of the specimen and since this stress drives creep deformation, the rate of creep deformation is high (Fig. 10a). The maximum principle stress, σ_1, is low directly adjacent to the punch. However a combination of high radial and hoop stresses results in high σ_1 on the underside of the disc centre (Fig. 10b). Then, as punch displacement increases, the stress field evolves and the peak stress decreases and moves away from the centre of the disc. Beyond punch displacements of approx. 1.3 mm, stress increases as the disc begins to thin causing an increase in displacement rate.

The model predicts that displacement rates are high during the initial part of the test with the rate decreasing to a minimum value at approximately $0.5t_F$ where t_F is the time to rupture. This decreasing displacement rate, as shown in Fig. 13, is evident despite little primary creep being observed during uniaxial creep in γ-TiAl at 700 °C and 750 °C. It is interesting to note that displacement/time plots for γ-TiAl SP tests have much different shapes than creep curves obtained from uniaxial creep testing. The SP curves display an extended period of time during which the displacement rate decreases (Fig. 4a), whereas uniaxial creep curves for γ-TiAl display little primary creep (Fig. 4b). An explanation for this behaviour can be obtained from stress analyses of the

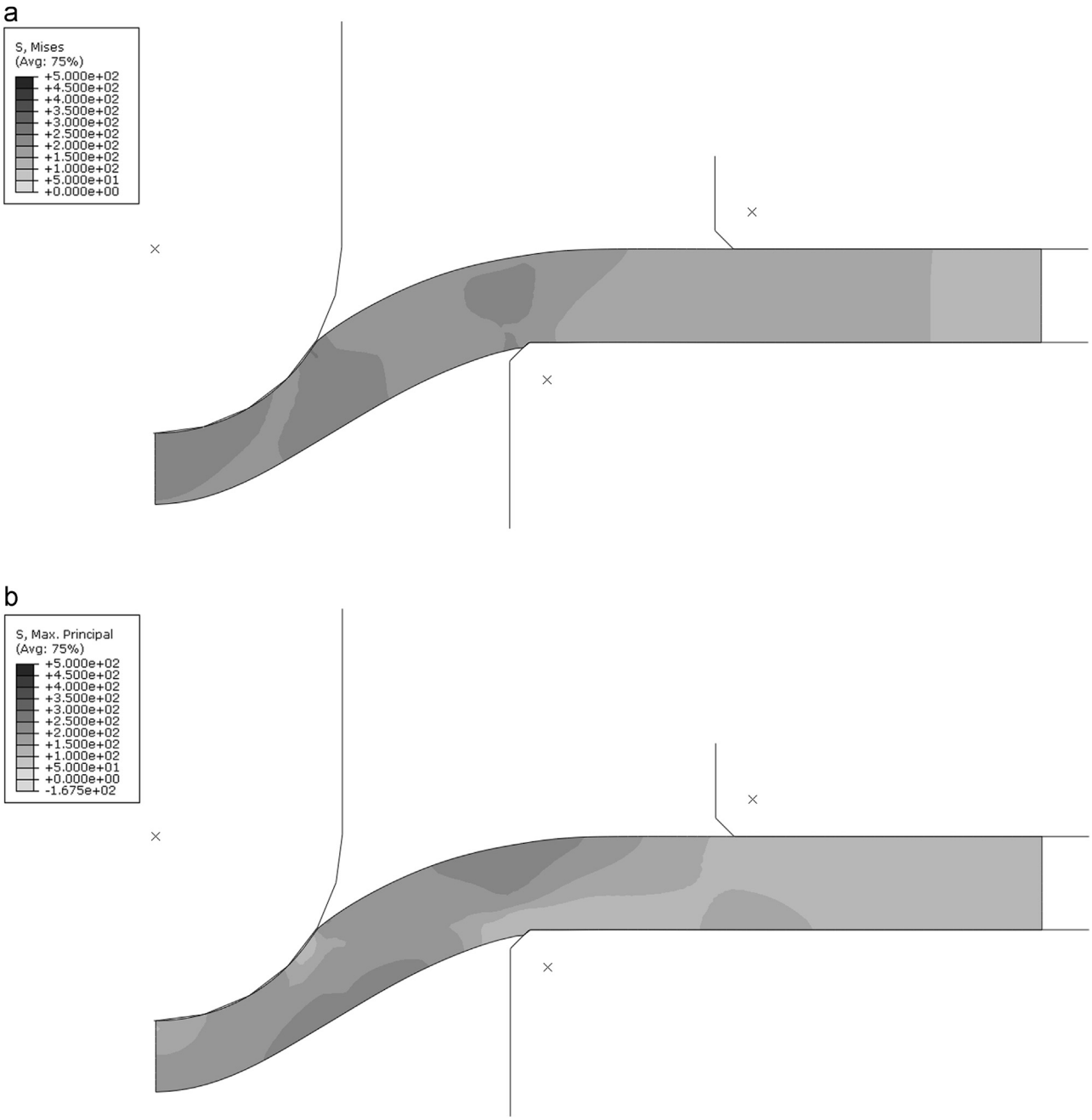

Fig. 12. Predicted (a) von-Mises and (b) maximum principle stress in the disc with a punch displacement of 1.0 mm and a punch load of 254 N (700 °C).

SP test (Figs. 10–12). These show that stress is initially high in the centre of the disc due to bending but decreases as punch displacement increases. Therefore the pseudo primary creep observed during the SP test can be attributed to the evolving stress in the disc, as opposed to uniaxial primary creep due which is attributed to dislocation hardening mechanisms. These curves were generated assuming that no creep rupture occurs and display much longer lives than those observed experimentally. Small punch creep curves terminate abruptly with a rapid increase in displacement rate (Figs. 4a and 5) whereas the predicted displacement rates shown in Fig. 13 indicated a gradual increase in rate prior to rupture. Furthermore Fig. 7 clearly shows that cracking occurs during the early stages of the SP test and therefore a better representation of the SP test can be made using a model for creep fracture in γ-TiAl.

4.4. Creep damage and rupture in the SP creep test

The above predictions were made without using a rupture criterion. Creep damage has been predicted using a continuum creep damage parameter W, which represents microstructural instabilities due to tertiary creep [21]. The material is assumed to fracture as W exceeds a critical value, W_{crit}, which is calculated from uniaxial creep rupture data and can be related to stress (σ) using

$$W_{crit} = c + \ln\left(\frac{\sigma}{\sigma_{TS}}\right)k \tag{18}$$

where c and k are material constants [16]. This model is applied to the problem of SP creep in γ-TiAl by reducing element stiffness as W exceeds W_{crit} at each Gauss point in each element. Reducing the

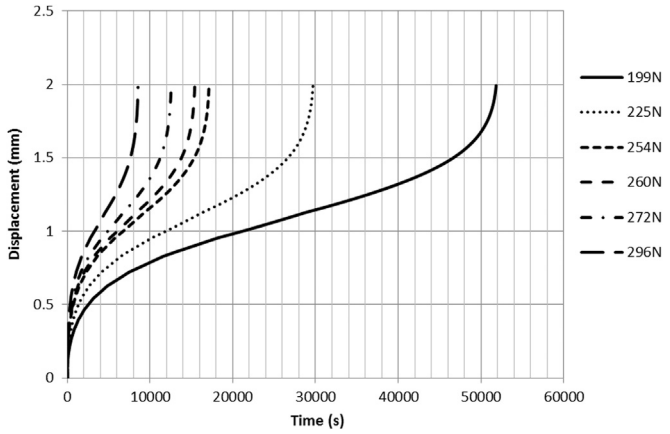

Fig. 13. Predicted SP creep displacement–time curves (700 °C).

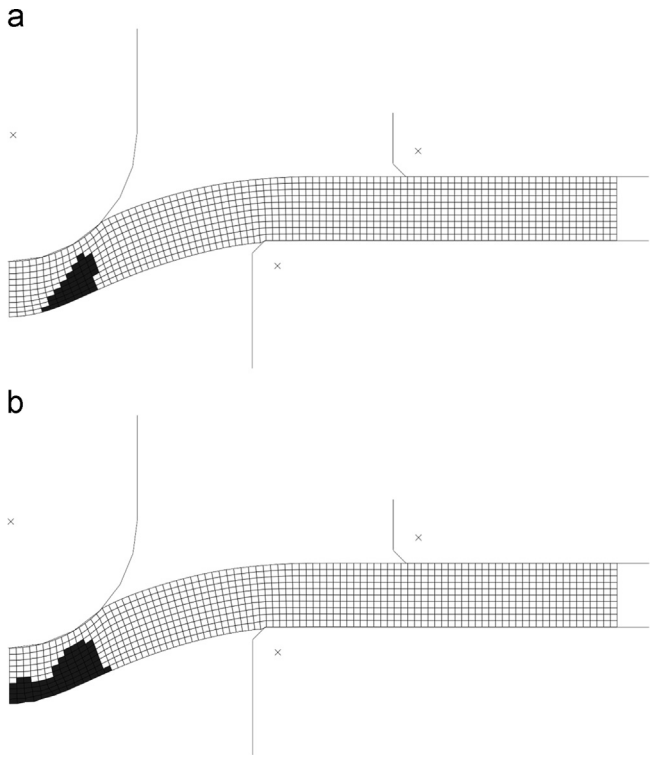

Fig. 14. Predicted path of material failure at 750 °C with a punch load of 235 N with rupture criteria based on (a) von-Mises stress, $\bar{\sigma}$ and (b) maximum principle stress, σ_1

stiffness redistributes the stress to the surrounding elements, simulating the effect of cracking. Therefore, using this rupture criterion in the SP creep model, predictions of miniature disc failure can be made. Eq. (18) is derived from uniaxial tensile creep tests where the applied stress, $\sigma = \bar{\sigma} = \sigma_1$. Since the stress in the SP test is multiaxial and evolves with time, σ in Eq. (18) must be substituted with a suitable component of stress. If rupture is based on von-Mises stress, $\bar{\sigma}$, then the onset of failure occurs away from the disc centre indicating the initiation of a circular crack (Fig. 14a). However, if σ is substituted with σ_1 in Eq. (18) then the model predicts that rupture will initiate at the disc centre (Fig. 14b) and that element failure occurs very early in the test, consistent with experimental observations. As the SP creep test continues this concentrated region of failed elements expands. Since the creep model uses implicit time integration, the point at which the failed elements extend across the thickness of the disc causes instability in the stiffness matrix and the model cannot continue. Initial displacement rates predicted using the rupture criterion (Eq. 18) are similar to those predicted without.

Interrupted SP creep tests revealed that cracks formed early in the experiment and were found to initiate in the centre of the disc, propagating radially. This is in contrast to the failure of many other alloys which fail around the periphery of the punch under an applied SP load. Furthermore, this is inconsistent with uniaxial creep tests on this alloy where large creep ductilities (up to 34%) are typically observed over this temperature range [4]. Stress analyses reveal that cracks in the γ-TiAl SP discs form where σ_1 is greatest and when this component of stress is high early in the test. SP creep tests on ductile alloys fail where $\bar{\sigma}$ is high [20] however cracking occurs in the latter stages of the test. Substituting σ_1 into Eq. (18) results in predictions of material failure consistent with the onset of cracking observed experimentally for this alloy. Therefore, it can be deduced that the SP creep behaviour of this γ-TiAl alloy is strongly dependent on the maximum principle stress, σ_1. Previous studies have shown that tertiary creep in this alloy initiates due to microstructural instabilities [16], such as strain incompatibilities between lamellar grains [23], with uniaxial creep fracture surfaces displaying interlamellar and intergranular cracking [4]. Therefore, the nature of the cracking and the dependence of this alloy on σ_1 indicate that the lamellar microstructure strongly influences the SP creep behaviour, with rupture a result of microstructural degradation such as the consolidation of inter-lamellar cracks.

5. Conclusions

Displacement verses time curves for γ-TiAl SP tests have a different shape to those observed from more conventional uniaxial approaches due to the evolution of the stress state in the SP test, not some micromechanical phenomenon. Furthermore, interrupted tests have shown that cracking occurs early in the γ-TiAl SP creep test and that these cracks initiate in the centre of the disc and propagate in a radial manner. This is contradictory to the deformation behaviour of SP tests on more ductile alloys where disc failure occurs late in the test with a radial fracture. This mode of fracture contributes to a load dependence which is different to that obtained from uniaxial testing resulting in stress rupture curves with different gradients. Consequently, the k_{SP} correlation is limited in its application and fails to represent the two sets of rupture data. However, the SP method still provides an effective tool for establishing the representative creep behaviour of the material at different temperatures and across different load conditions where only limited material quantities are available.

Stress analyses of the SP creep test reveal that the stress evolves during the test, with the peak maximum principle stress occurring on the underside of the disc during the early stages of creep. However, the location of the peak stress changes during the test. A damage model dependent on σ_1 predicts rupture consistent with experimental observations, indicating that rupture is a result of a microstructural degradation such as interlamellar and intergranular cracking.

Acknowledgments

The current research was funded under the EPSRC Rolls-Royce Strategic Partnership in Structural Metallic Systems for Gas Turbines (grants EP/H500383/1 and EP/H022309/1).

References

[1] L. Zhang, G. Qiu, J. Wu, Scr. Metall. Mater. 32 (10) (1995) 1683–1688.
[2] X. Wu, Intermetallics 14 (10-11) (2006) 1114–1122.
[3] S.W. Kim, J.K. Hong, Y.S Na, J.T. Yeom, S.E. Kim, Mater. Des. 54 (2014) 814–819.
[4] Z. Abdallah, M.T. Whittaker, M.R. Bache, Intermetallics 38 (2013) 55–62.
[5] J. McBride, S. Malinov, W. Sha, Mater. Sci. Eng. A 1-2 (2004) 129–137.
[6] K.Y. Won, Mater. Sci. Eng. A 192–193 (1995) 519–533.
[7] M. Thomas, M.P. Bacos, High Temp. Mater. 3 (2011) 1–11.
[8] F. Dobes, K. Milička, Mater. Charact. 59 (2008) 961–964.
[9] K. Turba, R.C. Hurst, P. Hahner, J. Nucl. Mater. 428 (1–3) (2012) 76–81.
[10] F. Hou, H. Xu, Y. Wang, L. Zhang, Eng. Fail. Anal. 28 (2013) 215–221.
[11] F. Dobes, K. Milicka, Mater. Sci. Eng. A 36 (2002) 245–248.
[12] D. Blagoeva, Y.Z. Li, R.C. Hurst, J. Nucl. Mater. 409 (2) (2011) 124–130.
[13] Y. Li, R. Sturm, Mater. High Temp. 23 (3-4) (2006) 225–232.
[14] R.C. Hurst, R.J. Lancaster, G. Norton, R. Banik, M.R. Bache, A Renaissance in Small Punch testing at Swansea University, Baltica IX, VTT Technology, Helsinki, 11–13 June 2013, p. 106.
[15] CEN Workshop Agreement, CWA 15627:2006 E, Small Punch Test Method for Metallic Materials, CEN, Brussels, 2006.
[16] W. Harrison, Z. Abdallah, M. Whittaker, Materials 7 (2014) 2194–2209.
[17] ISO204:2009, Metallic Materials – Uniaxial Creep Testing in Tension – Method of Test.
[18] G. Norris, Power House, ⟨http://www.flightglobal.com/news/articles/power-house-207148/⟩[accessed 13.06.06].
[19] R.W. Evans, M. Evans, Mater. Sci. Technol. 22 (2006) 1155–1162.
[20] K.I. Kobayashi, I. Kajihara, H. Koyama, G.C. Stratford, J. Solid Mech. Mater. Eng. 4 (2010) 75–86.
[21] R.W. Evans, Proc. R. Soc. A Math. Phys. Eng. Sci. 456 (2000) 835–868.
[22] W.J. Harrison, M.T. Whittaker, C. Deen, Mater. Res. Innov. 17 (2013) 323–326.
[23] J. Beddoes, L. Zhao, P. Au, D. Dudzinsky, J. Triantafillou, Structural Intermetallics 1997, in: M.V. Nathal, R. Darolia, C.T. Liu, P.L. Martin, D.B. Miracle, R. Wagner, M. Yamaguchi (Eds.), TMS, Warrendale, PA, USA, 1997.